Experimental observation of metallic states with different dimensionality in a quasi-one-dimensional charge density wave compound

P. Rezende-Gonçalves [1,2,*] M. Thees,[1] J. Rojas-Castillo [3] D. Silvera-Vega,[3] R. L. Bouwmeester [4] E. David [1] A. Antezak [1] A. J. Thakur [1] F. Fortuna [1] P. Le Fèvre [5] M. Rosmus [6] N. Olszowska [6] T. Sobol [6] R. Magalhães-Paniago [2] A. C. Garcia-Castro [7] P. Giraldo-Gallo [3] E. Frantzeskakis [1,†] and A. F. Santander-Syro [1,‡]

[1]*Université Paris-Saclay, CNRS, Institut des Sciences Moléculaires d'Orsay, 91405 Orsay, France*

[2]*Departamento de Física, Universidade Federal de Minas Gerais, Av. Pres. Antonio Carlos, 6627 Belo Horizonte, Brazil*

[3]*Department of Physics, Universidad de Los Andes, Bogotá 111711, Colombia*

[4]*Faculty of Science and Technology and MESA+ Institute for Nanotechnology, University of Twente, 7500 AE Enschede, Netherlands*

[5]*Synchrotron SOLEIL, L'Orme des Merisiers, Saint-Aubin-BP48, 91192 Gif-sur-Yvette, France*

[6]*National Synchrotron Radiation Centre SOLARIS, Jagiellonian University, Czerwone Maki 98, 30-392 Kraków, Poland*

[7]*School of Physics, Universidad Industrial de Santander, Carrera 27 Calle 09, 680002 Bucaramanga, Colombia*

(Received 18 July 2023; revised 11 June 2024; accepted 23 July 2024; published 25 September 2024)

$TaTe_4$ is a quasi-one-dimensional tetrachalcogenide that exhibits a charge density wave (CDW) instability caused by a periodic lattice distortion. Recently, pressure-induced superconductivity has been achieved in this compound, revealing a competition between these different ground states and making $TaTe_4$ very interesting for fundamental studies. Although $TaTe_4$ exhibits CDW ordering below 475 K, transport experiments have reported metallic behavior with a resistivity plateau at temperatures lower than 10 K. In this paper, we study the electronic structure of $TaTe_4$ using a combination of high-resolution angle-resolved photoemission spectroscopy and density functional calculations. Our results reveal the existence of the long-sought metallic states. These states exhibit mixed dimensionality, while some of them might have potential topological properties.

DOI: 10.1103/PhysRevB.110.125151

I. INTRODUCTION

Since the discovery of new topological phases of matter in the last decade [1,2], the general classification of the electronic structure of solids has been largely enriched. Topological insulators [3–5], superconductors [6,7], and an extended set of remarkable materials [8–11] have made condensed matter physics much more complex. Because of their technological potential [12–15], the investigation of novel materials is crucial [16]. In this context, transition metal chalcogenides (TMCs) stand out for their diversity and versatility [17,18]. The binary combination of a transition metal and an element from the chalcogen family (S, Se, or Te) produces, in most cases, a layered compound that foments the appearance of interesting physical properties related to low dimensionality [19,20].

A notable example of materials with intriguing properties induced by low dimensionality is the family of quasi-one-dimensional (quasi-1D) transition metal chalcogenides. These compounds are known for their crystalline structure formed by linear chains of transition metal atoms surrounded by chalcogen atoms [21–23]. This peculiar arrangement has important implications for the electronic transport in those compounds, producing effects that should be observed in a theoretical one-dimensional crystal, such as charge density waves (CDWs) [24–26]. This is the case for the tellurides $NbTe_4$ and $TaTe_4$, both of which exhibit charge density ordering below room temperature [27,28]. Recently, pressure-induced superconductivity has also been reported for both compounds [29,30], demonstrating the interplay between these two nontrivial ground states.

Furthermore, $TaTe_4$ has been predicted to exhibit topological properties related to the existence of degeneracy points in its band structure, referred to as Dirac nodes [31]. In addition, magnetotransport experiments have revealed the metallic behavior of $TaTe_4$ with a field-induced metal-to-insulator transition at about 35 K, followed by a resistivity plateau below 10 K [32,33]. In nonmagnetic systems [34], a resistivity plateau can be a fingerprint of low-dimensional states, including topological surface states, where the presence of protected metallic surface states saturates the bulk insulating resistivity at low temperatures [35,36]. The same feature is observed in topological semimetals when exposed to magnetic fields [37,38], but the underlying mechanism is still under debate.

The coexistence of 1D and three-dimensional (3D) electronic bands in $TaTe_4$ has been revealed more than 20 years ago through angle-resolved photoemission spectroscopy (ARPES) measurements, albeit no metallic states (i.e., no states crossing the Fermi level) were observed [39]. Theoretically, in quasi-1D materials, the photoemission intensity vanishes at the chemical potential and no Fermi level cutoff

*Contact author: pedro.rezende-goncalves@universite-paris-saclay.fr

†Contact author: emmanouil.frantzeskakis@universite-paris-saclay.fr

‡Contact author: andres.santander-syro@universite-paris-saclay.fr

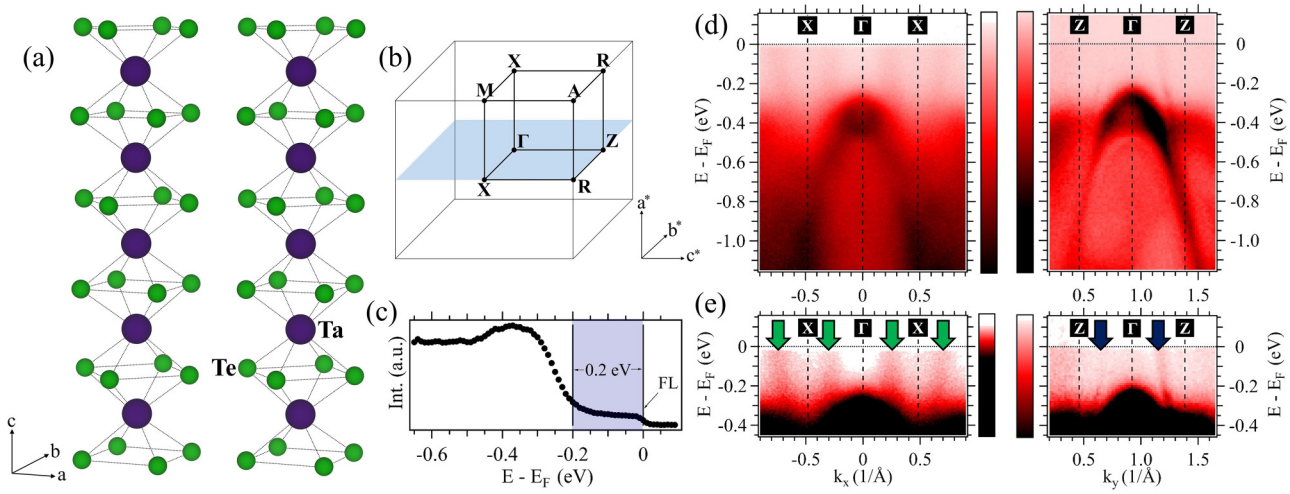

FIG. 1. (a) Crystal structure of $TaTe_4$ showing the Ta linear chains and the regular octahedra formed by Ta and the Te squares. Ta and Te atoms are represented by purple and green spheres, respectively. (b) Reciprocal unit cell of $TaTe_4$ and the corresponding high-symmetry points. The measurement plane perpendicular to the a^* axis is highlighted. (c) Angle-integrated intensity map of $TaTe_4$ showing the Fermi level cutoff and the suppression of spectral intensity in an energy window of 0.2 eV. (d) ARPES energy-momentum maps of $TaTe_4$ along Γ-X and Γ-Z, showing the dispersion perpendicular and parallel to the linear chains, respectively. (e) Energy-momentum maps along Γ-X and Γ-Z with saturated contrast over the region of reduced spectral intensity, showing electronlike metallic states (indicated by green arrows) and a holelike metallic state (indicated by blue arrows) crossing the Fermi level. The Brillouin zone boundaries are marked by dashed lines in all ARPES images. All measurements were carried out with a photon energy of 75 eV and linear-horizontal (LH) polarization.

is expected [40,41]. In contrast, $TaTe_4$ exhibits a well-defined Fermi level cutoff within a region of reduced spectral weight ranging from the Fermi level down to about -0.2 eV. Although optical conductivity measurements [39] indicate the presence of free carriers near the Fermi level, in addition to the metallic character revealed by transport measurements, no dispersive states have been observed in this region. The apparent inconsistency regarding the existence and nature of metallic states in $TaTe_4$ calls for a new experimental investigation of its band structure.

In this work we provide insights into the electronic band structure of $TaTe_4$ by means of high-resolution ARPES and density functional calculations (DFT). We experimentally probe the long-sought metallic states that cross the Fermi level. Some of these experimentally resolved states form 3D Fermi surface contours, while others exhibit quasi-1D features.

II. MATERIALS AND METHODS

A. Sample growth

Single crystals of $TaTe_4$ were grown by the self-flux method [42]. Alumina crucibles containing mixtures of 1 mol% elemental Ta and 99 mol% elemental Te powders were placed in an evacuated, sealed quartz tube. The mixture was heated in a box furnace up to 700 °C and kept at this temperature for 12 h. The temperature was then gradually decreased to 500 °C at a rate of 2 °C/h. The containers were quickly transferred to a centrifuge, where the $TaTe_4$ crystals were separated from the remaining melt. Once at room temperature, silver-colored rectangular crystals with dimensions up to $0.1 \times 0.1 \times 1$ cm^3 were obtained. The formation of a single-crystalline phase was confirmed by x-ray diffraction (see Sec. I of the Supplemental Material [43]).

B. Experimental methods

ARPES measurements were carried out using hemispherical electron analyzers with vertical slits at the CASSIOPEE beamline of Synchrotron SOLEIL (France) and URANOS and PHELIX beamline of Synchrotron SOLARIS (Poland). In order to generate pristine surfaces, $TaTe_4$ crystals were cleaved *in situ*, exposing the (100) crystalline plane. Typical resolutions in electron energy and angle were 15 meV and 0.25°, in all experimental setups. ARPES measurements were performed at temperatures not higher than 20 K and pressure below 5×10^{-11} mbar. Measurements with a photon energy of 75 eV correspond to a measurement plane right across the center of the bulk Brillouin zone [i.e., blue plane highlighted in Fig. 1(b)] assuming an inner potential of 18 eV (see Sec. III of the Supplemental Material [43] for details).

C. Theoretical and computational approach

Theoretical analyses were performed within the framework of first-principles calculations in the density-functional theory (DFT) [44,45] approach. The mentioned calculations were carried out in the Vienna *ab initio* simulation package, VASP code (version 5.4.4) [46,47]. The projected-augmented waves approach (PAW [48]) was employed to represent the valence and core electrons. The electronic configurations considered in the pseudopotentials as valence electrons are Ta: ($5p^6 6s^2 5d^3$, version 07Sep2000) and Te: ($5s^2 5p^4$, version 08April2002). The exchange correlation was represented within the generalized gradient approximation (GGA-PBEsol) parametrization [49]. The periodic solution of the crystal was represented by using Bloch states with a Monkhorst-Pack [50] k-point mesh of $13 \times 13 \times 13$ in the high-symmetry $P4/mcc$ (SG. 124) phase and scaled to $9 \times 9 \times 5$ in the low-symmetry CDW $P4/ncc$ (SG. 130) phase

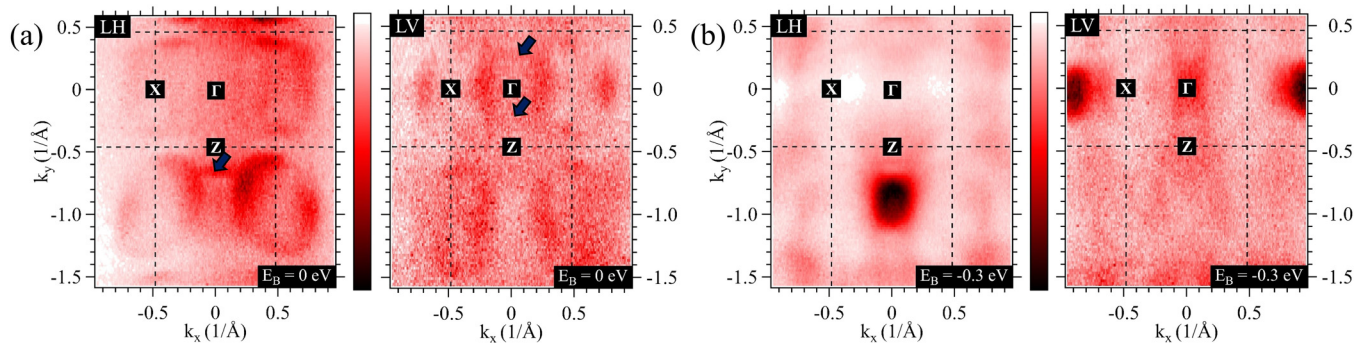

FIG. 2. (a) ARPES in-plane Fermi surface maps ($E_B = 0$) of $TaTe_4$ obtained with photons of linear horizontal (LH, left panel) and linear vertical (LV, right panel) polarization, showing the in-plane contours of the electronlike metallic states (elliptical contours) and of the quasi-1D features (indicated by arrows). (b) ARPES constant energy maps of $TaTe_4$ at $E_B = -0.3$ eV obtained in both polarizations (LH on the left and LV on the right), showing the contours at the band maximum of the holelike states centered at Γ. The Brillouin zone boundaries are marked by dashed lines in all images. All measurements were carried out with a photon energy of 75 eV.

into the $2 \times 2 \times 3$ supercell representation. We used a 600-eV energy cutoff to ensure forces convergence of less than 0.001 eV $Å^{-1}$ and energy less than 0.1 meV. Spin-orbit coupling (SOC) effect was considered as implemented in the VASP code [51]. To analyze the electronic structure, we made use of the PYTHON library PYPROCAR [52]. To estimate the surface states, we utilized the Wannier functions methodology, for which the wannierization was performed using the WANNIER90 code [53,54] and postprocessed with the WANNIERTOOLS package [55]. For the Wannierization process, p orbitals for Te atoms whereas the d orbitals were considered for Ta sites. Finally, the structural figures illustrations were performed with the VESTA code [56].

III. RESULTS AND DISCUSSIONS

The crystal structure of $TaTe_4$ [57] consists of linear chains of Ta atoms surrounded by Te atoms, with each atom representing a vertex of a regular octahedron. The underlying square bases are rotated by 45° with respect to each other, resulting in an antiprismatic configuration [Fig. 1(a)]. The high symmetry (in the non-CDW phase) unit cell is the tetragonal $P4/mcc$ (SG 124) with lattice parameters $a = b = 6.514$ Å and $c = 6.809$ Å, where the major axis is oriented parallel to the chains. The reciprocal unit cell is shown in Fig. 1(b). The natural cleavage plane is perpendicular to a (or equivalently b), hence the measurements plane is defined by the b and c axes (or equivalenty a and c axes). Lattice distortions in $TaTe_4$, driven by a V_4 mode as in the $NbTe_4$ case [28], are responsible for a CDW transition at $T = 475$ K that leads the system into a commensurate $2 \times 2 \times 3$ $P4/ncc$ structure [27]. Both crystal structures are shown in Sec. II of the Supplemental Material [43]. Although the atomic structure of $TaTe_4$ has been known for many years, its electronic band structure is still not fully understood.

A. Electronic band structure by ARPES

According to the electronic configuration of Ta and Te atoms, the unpaired electrons must be located in the Ta-5d and Te-5p shells, and their hybridization results in the band structure of $TaTe_4$ near the Fermi level [58]. In-plane ARPES measurements show that the electronic structure near the Fermi level consists of a holelike band centered at the Γ point and an electronlike band centered at the X point [Fig. 1(d)]. The spectral intensity is significantly reduced near the Fermi level, a particular interesting character of $TaTe_4$, which might be related to the CDW gap opening. The width of the region of reduced spectral weight is around 0.2 eV [Fig. 1(c)]. In contrast to Zwick and coworkers [39], our measurements distinctly show metallic states crossing the Fermi level [see Fig. 1(e)]. The observation of these states in the aforementioned region of reduced spectral weight solves the alleged mystery of $TaTe_4$ exhibiting metal-like resistivity curves [32] without any, so far, experimental fingerprint of a metallic state [39].

The electronlike band around X gives rise to elliptical electron pockets that are the most readily observable features of the Fermi surface contours. The corresponding Fermi surface maps shown in Fig. 2(a) are obtained using two photon polarizations: linear horizontal (LH) and linear vertical (LV). The spectral weight of the Fermi contours is strongly influenced by the crystal orientation, as manifested by the lack of symmetry between adjacent Brillouin zones, and by the polarization of incoming photons. This influence is due to photoemission matrix elements, which are responsible for enhancing or attenuating the spectral signal of different wave functions [59–61]. The effect of the photon polarization is also shown in Sec. IV of the Supplemental Material [43]. The dispersion of the metallic states is reminiscent of the Dirac-type dispersion of surface states reported for several materials, including topological insulators [62–64]. Nevertheless, before drawing any conclusion on the origin of these states, their dimensionality will be further discussed in a later section by means of photon-energy-dependent ARPES and through comparison to DFT calculations. We note that the lower-lying electronic states of $TaTe_4$ are also subject to strong photoemission matrix elements effects as revealed by the contours of the band maximum of the holelike state centered at the Γ point [Fig. 2(b)].

We now draw the readers' attention to the holelike metallic state crossing the Fermi level along Γ-Z [Fig. 1(e), right panel]. This state corresponds to quasi-1D Fermi surface features which are pointed out by arrows in Fig. 2(a). This means that it poorly disperses along any direction normal

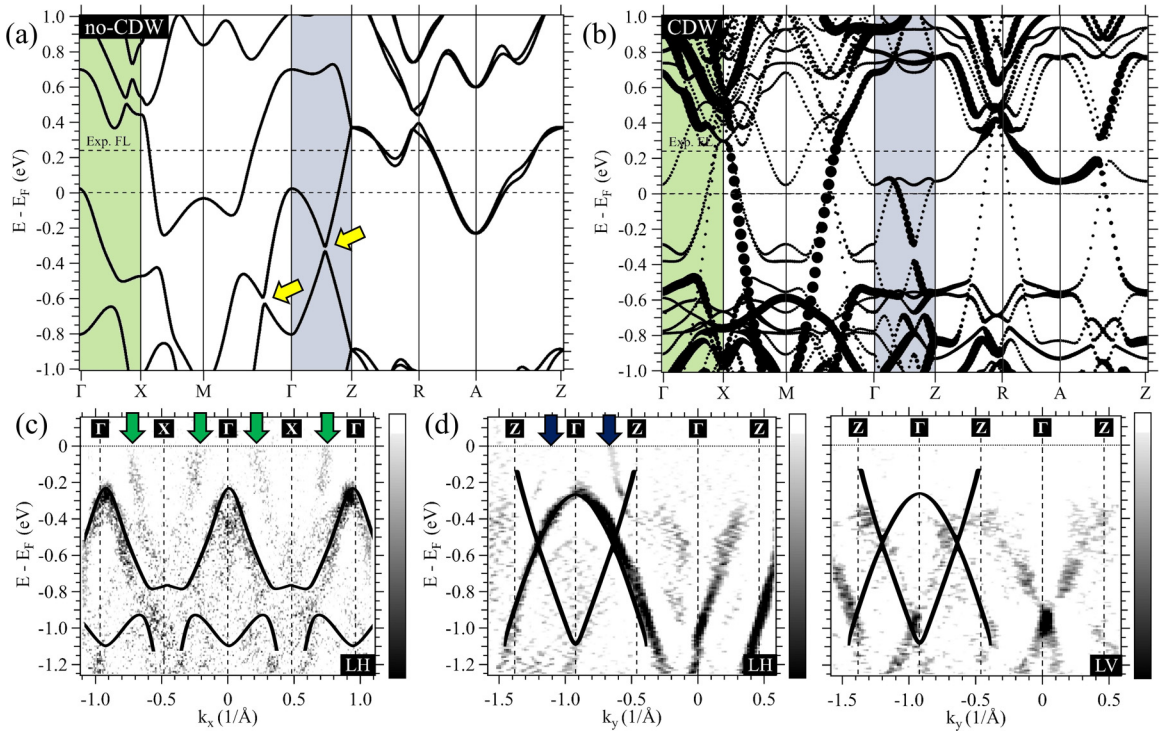

FIG. 3. (a) Electronic band structure of $TaTe_4$ calculated by DFT in the unmodulated phase with SOC. The yellow arrows point the two predicted band crossings near the Fermi level. (b) Electronic band structure of $TaTe_4$ calculated by DFT in the CDW-modulated phase folded into the $1 \times 1 \times 1$ unit-cell reference of the unmodulated structure without SOC due to computational and theoretical limitations. Note: The marker size emulates the spectral weight of the bands. (c) Comparison between ARPES dispersion and DFT calculations in the unmodulated phase along Γ-X, showing the predicted holelike state centered at Γ and the electronlike metallic states (indicated by green arrows) not predicted by the calculations. (d) Comparison between ARPES dispersions and DFT calculations in the unmodulated phase along Γ-Z for both polarizations, showing the dispersion of the holelike state centered at Γ, visible only with horizontal polarization, and the electronlike state, visible only with vertical polarization. The quasi-1D feature is indicated by blue arrows. The calculated band structure in the non-CDW phase was shifted 0.24 eV in order to achieve a better agreement between theory and experiment. All measurements were carried out with a photon energy of 75 eV, and the energy-momentum maps were processed using the curvature method [67] to enhance the intensity of weak spectral features.

to the Γ-Z high-symmetry line. In terms of spectral intensity, the most intense quasi-1D feature is observed at $k_y = -0.64$ Å^{-1} in the LH Fermi surface map, while weaker features are found at $k_y = \pm 0.26$ Å^{-1} and $k_y = -0.26$ Å^{-1} in the LV Fermi surface map. The asymmetric intensity distribution observed on different in-plane Fermi surface maps is again a manifestation of the photoemission matrix elements [59–61]. We further note the much narrower spectral width of the holelike metallic states along Γ-Z, in comparison to the electronlike bands along Γ-X [compare left and right panels of Fig. 1(e)]. Narrower spectral widths are a common characteristic of surface-derived features. In the following section, we will further discuss the electronic structure of $TaTe_4$ through a comparison of the experimental results with DFT calculations.

B. Electronic band structure by DFT

The electronic band structure of $TaTe_4$ was calculated using first-principles calculations within the density-functional theory framework for two types of atomic structures: the unmodulated (i.e., undistorted) phase ($1\times1\times1$ – $P4/mcc$) and the CDW modulated (i.e., distorted) phase ($2\times2\times3$ – $P4/ncc$) folded into the $1 \times 1 \times 1$ unit-cell reference of the nonmodulated structure. The resulting band structures are shown in Figs. 3(a) and 3(b). Here, it is worth mentioning the relevance of the folded band structure chosen to represent the CDW-modulated phase. Considering $2 \times 2 \times 3$ structure without band folding, $TaTe_4$ shows a strongly metallic behavior [31,58], nonetheless, as the distortion, associated with the CDW phonon, is introduced into the reference symmetry a reduction on the bands crossing the Fermi level and a decrease on the density of state is expected. The latter suggests an apparent contradiction in the expected effect of a CDW modulation. The importance of the correlation between the structure distortions and the folded band electronic structure to the undistorted reference has been also highlighted in other works [65,66]. The method employed on that kind of calculation has an extra advantage: it provides an approximation of the spectral weight of the folded bands. The $TaTe_4$ folded calculation results on several bands with weak spectral weight crossing the Fermi level, reminiscent of the $2 \times 2 \times 3$ structure. There are two relevant bands with stronger spectral weights: one electronlike state centered around the M point, a high-symmetry point that is not contained in our plane of measurements, and the already-mentioned holelike state along Γ-Z. In fact, the folded calculation results on a gap opening

of this state, a point that will be important in later discussions. Although $TaTe_4$ lies in the CDW phase in the temperature range of our measurements, we observed no clear signs of band folding. As a matter of fact, and as it will become clear in the following, the band structure of the unmodulated phase describes more accurately our experimental results.

A comparative analysis between the electronic bands observed by ARPES and those predicted by DFT calculations was performed by superimposing of the calculated dispersions of the non-CDW phase on the energy-momentum maps along Γ-X and Γ-Z [Figs. 3(c) and 3(d)]. We obtained a very good agreement of theory and experiment after a rigid energy shift of the calculated band structure by 0.24 eV to higher binding energies. All the main features of the experimental band structure can find a counterpart in the theoretical bands with the sole exception of the metallic states discussed in the previous sections and pointed out by arrows in Figs. 3(c) and 3(d). In particular, along Γ-X, the holelike state with a maximum at -0.2 eV is captured by theory, while there are experimental traces of the lower-lying theoretical bands. On the other hand, along Γ-Z, one needs to consider the experimental maps measured using both photon polarizations (LH and LV) in order to observe all bands predicted by DFT. In our experimental configuration, LH photons are sensitive to the aforementioned holelike band while LV photons to an electronlike band with a minimum at around -1 eV. This extreme polarization dependence manifests itself very clearly in Fig. 2(b), and it is capable of completely suppressing the holelike state (i.e., the most intense feature of the entire spectrum) at the center of the first Brillouin zone (in case of LH photons) or in neighboring Brillouin zones (in case of LV photons). The different dependence of these bands on the photoemission matrix elements is an experimental confirmation of their different orbital origin. Indeed, the holelike band consists mainly of Te-5p orbitals while the electronlike band of Ta-5d_{z^2} orbitals [58]. We further note that while this electronlike band is predicted to cross the Fermi level, our results suggest that it instead bends down and forms a holelike maximum around the Z point of the Brillouin zone at approximately -0.4 eV: just as the other DFT bands it seems to avoid entering into the region of reduced spectral weight. If this region is related to the CDW as Zwick *et al.* inferred by comparison to their optical conductivity measurements [39], the experimentally observed band maximum along Γ-Z might be therefore an indirect fingerprint of the CDW.

We note, however, that the experimental bands do not match the DFT band structure of the CDW-modulated phase [Fig. 3(b)]. This observation might be surprising, but one has to consider that optical conductivity measurements have concluded that no more than 20%–30% of the charge carriers are involved in the CDW phase [39]. The folded CDW-phase calculation predicts the opening of several band gaps on the electronic band structure. Near the Fermi level, most of the bands are suppressed with the solemn exception of the bands in the path M-Γ-Z. Those bands have an important role regarding the topological aspects of $TaTe_4$. The folded calculation predicts the opening of band gaps on the accidental band crossings in Γ-M and Γ-Z, pointed by yellow arrows in Fig. 3(a). As will be discussed in the following section, these accidental crossings might be assigned to Dirac points, opening the possibility for the existence of axions in the material, as reported in the similar compound $(TaSe_4)_2I$ [68,69]. Last but not least, the fact that the metallic states lying in the region of reduced intensity have no counterpart in bulk calculations questions their attribution to bulk bands and calls for a determination of their dimensionality. In the following we will discuss in more detail the metallic states crossing the Fermi level by presenting experimental evidence that gives insights on their nature and origin.

C. Origin of the metallic states

As discussed previously, there are two sets of metallic states that cross the Fermi level: the states forming the elliptical electron pockets centered at X and those corresponding to the quasi-1D features normal to Γ-Z [Fig. 2(a)]. The former (latter) states are pointed by green (blue) arrows in Figs. 1–3. In order to verify the dimensionality of the states forming the elliptical contours, we have checked their out-of-plane dispersion by means of photon energy-dependent ARPES. The corresponding out-of-plane Fermi surface map of the elliptical electron pockets [Fig. 4(a)] clearly shows that they are three dimensional and follow the Brillouin zone periodicity. This experimental observation may come as a surprise for two reasons. First of all, they are not predicted by DFT calculations which should capture all three-dimensional bulk-derived states. Second, such dimensionality cannot explain the resistivity plateau seen in magnetotransport measurements [32,33], which is typical of low-dimensional states. On the other hand, the 3D character is in line with their broad spectral width in the in-plane measurements of Figs. 1 and 2. This observation is in contrast to the sharper quasi-1D features measured along Γ-Z, that will be the topic of the next paragraph. In order to get more information on the dimensionality of these states and the spatial extent of their associated wave functions, we invite future photoemission studies with bulk-sensitive probes (i.e., photons in the soft and hard x-ray regimes).

Moving forward, we will discuss the origin of the metallic states behind the experimentally resolved quasi-1D features. Unlike the three-dimensional metallic states discussed in the last paragraph, the quasi-1D features do not disperse in the plane that is normal to the sample surface [see Fig. 4(b)]. In other words, they represent surface states. As stated previously, in the unmodulated phase, both experiment (Fig. 1) and calculations (Fig. 3) agree that the band structure is dominated by a holelike band at Γ having a maximum at -0.2 eV. Moreover, there is an electronlike state [see Figs. 3(a) and 3(d)] crossing the holelike band at two points: along Γ-M and Γ-Z. As we will shortly explain, this interaction might be at the origin of the metallic quasi-1D features. Specifically, such accidental band crossings could evolve into Dirac points if they result from electronic bands with different symmetries [3,70]. The two bands in question have indeed different orbital symmetries as discussed in the frame of Fig. 3(d). The two alleged Dirac points are shown in Fig. 4(c). It is important here to note that whether or not a gap opening is observed, this could be a consequence of the calculation parameters, more specifically, the number of cells used in the calculations [71,72]. According to Zhang *et al.* there is a Dirac point along Γ-Z, while the band crossing along Γ-M results in a small

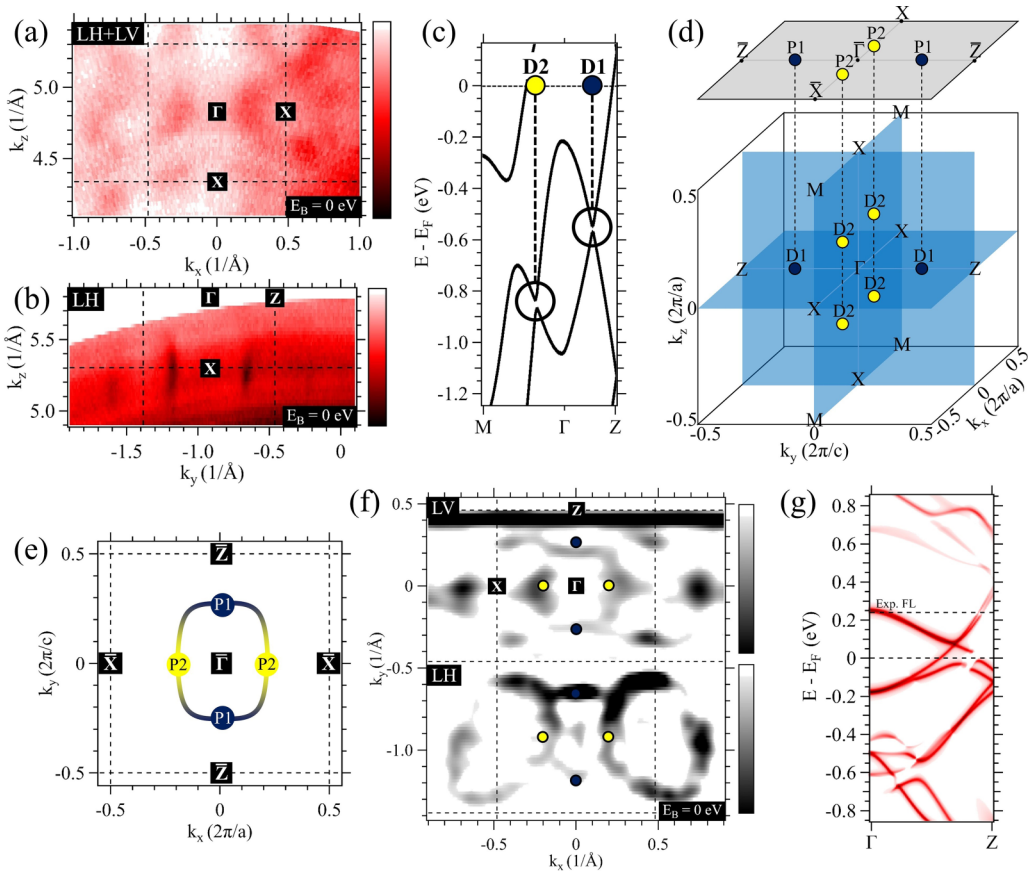

FIG. 4. (a) ARPES out-of-plane Fermi surface map ($E_B = 0$) of $TaTe_4$ obtained from the normal emission oriented along the in-plane direction Γ-X, superimposing the maps obtained using photons with both polarizations, showing the out-of-plane dispersion of the electronlike metallic states. The measurements were carried out using photon energies from 50 to 100 eV. (b) ARPES out-of-plane Fermi surface map ($E_B = 0$) of $TaTe_4$ obtained from the normal emission oriented along the in-plane direction Γ-Z using LH photons, showing the out-of-plane dispersion of the holelike metallic states (1D features). The measurements were carried out using photon energies from 70 to 110 eV. (c) Electronic band structure of $TaTe_4$ calculated by DFT along the M-Γ-Z direction, showing the band crossings along Γ-Z (blue) and Γ-M (yellow). The projections of the band crossings at the Fermi level are indicated by points D1 and D2, respectively. (d) Schematic of the positions of the points D1 and D2 in the reciprocal unit cell of $TaTe_4$ and their projections on the surface Brillouin zone indicated by P1 and P2. The indices 1 and 2 refer to a single and double projection, respectively. (e) Schematic of the positions of the points P1 and P2 on the surface Brillouin zone with a qualitative description of the Fermi arcs connecting them. (f) ARPES in-plane Fermi surface maps ($E_B = 0$) of $TaTe_4$ maps obtained with LH and LV polarization, and the superimposed expected k location of the Fermi arcs. This measurement was carried with a photon energy of 75 eV and the energy-momentum maps were processed using the curvature method [67] to enhance the intensity of weak spectral features. (g) Electronic dispersion of $TaTe_4$ calculated by bulk DFT (black lines) superimposed by the surface-sensitive dispersion calculated using Wannier functions (red lines) along the Γ-Z direction. The intensity of the red lines emulates the superficial character of the bands.

energy gap [31]. On the other hand, Guster *et al.* reported Dirac points in both band crossings [58]. In Sec. V of the Supplemental Material [43], we have computed the effect of the spin-orbit coupling (SOC) on these accidental band crossings. Although the SOC is responsible for breaking the degeneracy at band crossings and opening a band gap, the alleged Dirac points are protected by symmetry and remain intact, providing further evidence of their topological nature.

We now stress the fact that the intersection point between the electronlike and holelike bands was predicted to occur around $k_y = \pm 0.26$ Å^{-1} along Γ-Z, which matches perfectly with the k-space location of the quasi-1D features. This observation might provide a new explanation for the origin of these states since it is reminiscent of Fermi arcs associated with bulk Dirac points of 3D topological Dirac semimetals [73–75].

To examine the plausibility of the latter scenario, one must consider all the degeneracy points in the band structure of $TaTe_4$. Figure 4(c) shows the projection of the Dirac points along Γ-Z and Γ-M on the Fermi level, defining the points D1 and D2, respectively. In the reciprocal unit cell, six of these projected points are found: two D1 points at the intersection of the planes $k_z = 0$ and $k_x = 0$, referring to the Dirac points along Γ-Z; and four D2 points located at the plane $k_y = 0$, referring to the Dirac points along Γ-M [see Fig. 4(d)]. The in-plane ARPES measurements provide access to the plane $k_z = 0$, then it is necessary to address the projections of points D1 and D2 into this plane. The Fermi arcs associated with points P1 and P2 are shown schematically in Fig. 4(e) and they are superimposed onto the experimental Fermi surface map in Fig. 4(f). The result shows a decent agreement between the

experimentally observed quasi-1D features and the predicted positions of the Fermi arcs. Despite the fairly good agreement of our experimental findings with the scenario of Fermi arcs, one might be surprised that the bulk Dirac points lie at energies far from the immediate vicinity of the Fermi level, unlike Na_3Bi and Cd_3As_2 [73–75].

We also performed calculations using the Wannier representation for topological insulators [76] in order to examine the plausibility of the interpretation of the quasi-1D features as Fermi arcs. In Fig. 4(g), the dispersion relation along Γ-Z was obtained by this method. There are two relevant observations from Fig. 4(g). First of all, since the intensity of lines emulates the surface character of the bands, one concludes that the metallic band crossing the experimental Fermi level is essentially a surface state. Second, and most importantly, the band disperses to an accidental band crossing 0.16 eV below the experimental Fermi level. The crossing originated by this surface state may be ascribed to the Dirac point D1 since, no matter the method employed in the calculations, the accidental band crossing remains protected, even if there is no perfect quantitative match with the experimental values of energy and momentum. An extended analysis of the calculation using Wannier functions is presented in Sec. VI of the Supplemental Material [43]. On one hand, we stress once again that this is a rather tentative assignment of the quasi-1D features motivated by our experimental findings. On the other hand, recent calculations by Zhang and coworkers [31] have provided evidence that $TaTe_4$ should be indeed a topological semimetal making the existence of Fermi arcs highly possible. No matter the origin of the quasi-1D features, we note that their low dimensionality makes them likely candidates for being responsible for the resistivity plateau at low temperatures [32,33].

As a matter of fact, $TaTe_4$ possesses a unique band structure with metallic states of different dimensionality. Its peculiar Fermi surface consists of textbook 3D states, as well as quasi-1D features that may be part of contours of topological origin.

IV. SUMMARY AND CONCLUSIONS

In summary, our angle-resolved photoemission spectroscopy experiments on the charge density wave phase of the quasi-1D tetrachalcogenide $TaTe_4$ found that aside from the reduction of spectral weight near the Fermi level, there are no clear spectroscopic fingerprints of the CDW itself. On the other hand, our data revealed a well-defined Fermi surface made of various metallic states that had been unnoticed in previous photoemission studies [39]. Therefore, our work bridges the gap between spectroscopic studies on $TaTe_4$ and magnetotransport work [32,33] that had already reported clear metallic behavior. The metallic states of $TaTe_4$ have different dimensionality characters. Our study hints that the latter low-dimensional states might be part of Fermi arcs connecting the projections of band intersections. The potential existence of topological features in a quasi-1D compound combined with the opening of band gaps caused by the CDW distortion makes $TaTe_4$ an interesting material to study the relationship between topology, charge density waves, and axionic physics [11,68,69].

Note added. Recently, a preprint of a new photoemission study on $TaTe_4$ reported a similar band structure to the one in this paper [77]. Nevertheless, the authors attribute the quasi-1D features to backfolded contours of the 3D bulk states due to the periodicity of the CDW. In our data we have no signs of such a periodicity, and we further note that a CDW interpretation would necessarily mean that those features are purely 3D, a scenario that is incompatible with the lack of out-of-plane dispersion shown in Fig. 4(b) and their sharp spectral width. Moreover, in such case, these states could not be at the origin of the low-T resistivity plateau. In any case, this renewed interest in quasi-1D tetrachalcogenides calls for future studies with bulk-sensitive probes to clarify these issues.

ACKNOWLEDGMENTS

The authors acknowledge SOLEIL and SOLARIS for the provision of synchrotron radiation facilities, Proposals No. 20210251 (SOLEIL) and No. 212021 (SOLARIS). We would like to thank the beamline staff for their support during the experiment in beamline CASSIOPEE (SOLEIL) and URANOS/PHELIX (SOLARIS). Work at ISMO was supported by public grants from the French National Research Agency (ANR), project Fermi-NESt Grant No. ANR-16-CE92-0018, the "Laboratoire d'Excellence Physique Atomes Lumière Matière" (LabEx PALM project MiniVAN) overseen by the ANR as part of the "Investissements d'Avenir" program (reference: Grant No. ANR-10-LABX-0039), and CNRS International Research Project EXCELSIOR. We thank funding from Ministerio de Ciencias de Colombia, through the Grant No. 120480863414. P.R.-G. also received financial support from the Brazilian agency CAPES during his stay in ISMO under the process numbers 88887.370560/2019-00 (2020) and 88887.642783/2021-00 (2022). R.M-P. acknowledges support from CNPq and INCT-Nanocarbono. A.C.G.-C. acknowledges the support from the GridUIS-2 experimental test bed, developed under the Universidad Industrial de Santander (SC3-UIS) High Performance and Scientific Computing Centre, with support from UIS Vicerrectoría de Investigación y Extensión (VIE-UIS) and several UIS research groups, as well as other funding resources. A.C.G.-C. also acknowledges Grant No. 202303059C entitled Optimizacin de las Propiedades Termoeléctricas Mediante Tensión Biaxial en la Familia de Materiales $Bi_4O_4SeX_2$ (X = Cl, Br, I) Desde Primeros Principios supported by the LNS–BUAP.

[1] D. J. Thouless, M. Kohmoto, M. P. Nightingale, and M. den Nijs, Quantized Hall conductance in a two-dimensional periodic potential, Phys. Rev. Lett. **49**, 405 (1982).

[2] J. E. Moore, The birth of topological insulators, Nature (London) **464**, 194 (2010).

[3] M. Z. Hasan and C. L. Kane, *Colloquium:* Topological insulators, Rev. Mod. Phys. **82**, 3045 (2010).

[4] D. Hsieh, D. Qian, L. Wray, Y. Xia, Y. S. Hor, R. J. Cava, and M. Z. Hasan, A topological Dirac insulator in a quantum spin Hall phase, Nature (London) **452**, 970 (2008).

[5] Y. Xia, D. Qian, D. Hsieh, L. Wray, A. Pal, H. Lin, A. Bansil, D. Grauer, Y. S. Hor, R. J. Cava, and M. Z. Hasan, Observation of a large-gap topological-insulator class with a single Dirac cone on the surface, Nat. Phys. **5**, 398 (2009).

[6] J. G. Bednorz and K. A. Müller, Possible high T_c superconductivity in the Ba-La-Cu-O system, Z. Phys. B **64**, 189 (1986).

[7] A. Damascelli, Z. Hussain, and Z.-X. Shen, Angle-resolved photoemission studies of the cuprate superconductors, Rev. Mod. Phys. **75**, 473 (2003).

[8] A. Burkov, Topological semimetals, Nat. Mater. **15**, 1145 (2016).

[9] M. Sato and Y. Ando, Topological superconductors: A review, Rep. Prog. Phys. **80**, 076501 (2017).

[10] M. Dzero, J. Xia, V. Galitski, and P. Coleman, Topological Kondo insulators, Annu. Rev. Condens. Matter Phys. **7**, 249 (2016).

[11] A. Sekine and K. Nomura, Axion electrodynamics in topological materials, J. Appl. Phys. **129**, 141101 (2021).

[12] K. S. Novoselov, V. I. Fal'ko, L. Colombo, P. R. Gellert, M. G. Schwab, and K. Kim, A roadmap for graphene, Nature (London) **490**, 192 (2012).

[13] M. He, H. Sun, and Q. L. He, Topological insulator: Spintronics and quantum computations, Front. Phys. **14**, 43401 (2019).

[14] V. V. Kruglyak, S. O. Demokritov, and D. Grundler, Magnonics, J. Phys. D: Appl. Phys. **43**, 264001 (2010).

[15] G. A. Prinz, Magnetoelectronics applications, J. Magn. Magn. Mater. **200**, 57 (1999).

[16] M. L. Cohen and S. G. Louie, *Fundamentals of Condensed Matter Physics* (Cambridge University Press, Cambridge, 2016).

[17] K. Mitchell and J. A. Ibers, Rare-earth transition-metal chalcogenides, Chem. Rev. **102**, 1929 (2002).

[18] S. Manzeli, D. Ovchinnikov, D. Pasquier, O. V. Yazyev, and A. Kis, 2D transition metal dichalcogenides, Nat. Rev. Mater. **2**, 17033 (2017).

[19] A. Splendiani, L. Sun, Y. Zhang, T. Li, J. Kim, C.-Y. Chim, G. Galli, and F. Wang, Emerging photoluminescence in monolayer MoS_2, Nano Lett. **10**, 1271 (2010).

[20] H. Wang, X. Huang, J. Lin, J. Cui, Y. Chen, C. Zhu, F. Liu, Q. Zeng, J. Zhou, P. Yu, X. Wang, H. He, S. H. Tsang, W. Gao, K. Suenaga, F. Ma, C. Yang, L. Lu, T. Yu, E. H. T. Teo *et al.*, High-quality monolayer superconductor $NbSe_2$ grown by chemical vapour deposition, Nat. Commun. **8**, 394 (2017).

[21] A. Patra and C. S. Rout, Anisotropic quasi-one-dimensional layered transition-metal trichalcogenides: synthesis, properties and applications, RSC Adv. **10**, 36413 (2020).

[22] J. O. Island, A. J. Molina-Mendoza, M. Barawi, R. Biele, E. Flores, J. M. Clamagirand, J. R. Ares, C. Sánchez, H. S. J. van der Zant, and R. D'Agostag, Electronics and optoelectronics of quasi-1D layered transition metal trichalcogenides, 2D Mater. **4**, 022003 (2017).

[23] P. Gressier, M. Whangbo, A. Meerschaut, and J. Rouxel, Electronic structures of transition-metal tetrachalcogenides $(MSe_4)_nI$ (M = Nb, Ta), Inorg. Chem. **23**, 1221 (1984).

[24] G. Grüner, The dynamics of charge-density waves, Rev. Mod. Phys. **60**, 1129 (1988).

[25] G. Grüner, The dynamics of spin-density waves, J. Phys. C: Solid State Phys. **66**, 1 (1994).

[26] L. P. Gor'kov and G. Grüner, *Charge Density Waves in Solids* (North-Holland, Amsterdam, 1989).

[27] F. W. Boswell, A. Prodan, and J. K. Brandon, Charge-density waves in the quasi-one-dimensional compounds $NbTe_4$ and $TaTe_4$, J. Phys. C: Solid State Phys. **16**, 1067 (1983).

[28] J. A. Galvis, A. Fang, D. Jiménez-Guerrero, J. Rojas-Castillo, J. Casas, O. Herrera, A. C. Garcia-Castro, E. Bousquet, I. R. Fisher, A. Kapitulnik, and P. Giraldo-Gallo, Nanoscale phase-slip domain walls in the charge density wave state of the Weyl semimetal candidate $NbTe_4$, Phys. Rev. B **107**, 045120 (2023).

[29] X. Yang, Y. Zhou, M. Wang, H. Bai, X. Chen, C. An, Y. Zhou, Q. Chen, Y. Li, Z. Wang, J. Chen, C. Cao, Y. Li, Y. Zhou, Z. Yang, and Z.-A. Xu, Pressure induced superconductivity bordering a charge-density-wave state in $NbTe_4$ with strong spin-orbit coupling, Sci. Rep. **8**, 6298 (2018).

[30] Y. Yuan, W. Wang, Y. Zhou, X. Chen, C. Gu, C. An, Y. Zhou, B. Zhang, C. Chen, R. Zhang, and Z. Yang, Pressure-induced superconductivity in topological semimetal candidate $TaTe_4$, Adv. Electron. Mater. **6**, 1901260 (2020).

[31] X. Zhang, Q. Gu, H. Sun, T. Luo, Y. Liu, Y. Chen, Z. Shao, Z. Zhang, S. Li, Y. Sun, Y. Li, X. Li, S. Xue, J. Ge, Y. Xing, R. Comin, Z. Zhu, P. Gao, B. Yan, J. Feng *et al.*, Eightfold fermionic excitation in a charge density wave compound, Phys. Rev. B **102**, 035125 (2020).

[32] X. Luo, F. C. Chen, Q. L. Pei, J. J. Gao, J. Yan, W. J. Lu, P. Tong, Y. Y. Han, W. H. Song, and Y. P. Sun, Resistivity plateau and large magnetoresistance in the charge density wave system $TaTe_4$, Appl. Phys. Lett. **110**, 092401 (2017).

[33] Y. Gao, L. Xu, Y. Qiu, Z. Tian, S. Yuan, and J. Wang, Anisotropic large magnetoresistance in $TaTe_4$ single crystals, J. Appl. Phys. **122**, 135101 (2017).

[34] M. Pickem, E. Maggio, and J. M. Tomczak, Resistivity saturation in Kondo insulators, Commun. Phys. **4**, 226 (2021).

[35] Z. Ren, A. A. Taskin, S. Sasaki, K. Segawa, and Y. Ando, Large bulk resistivity and surface quantum oscillations in the topological insulator Bi_2Te_2Se, Phys. Rev. B **82**, 241306(R) (2010).

[36] D. Kim, J. Xia, and Z. Fisk, Topological surface state in the Kondo insulator samarium hexaboride, Nat. Mater. **13**, 466 (2014).

[37] S. Sun, Q. Wang, P.-J. Guo, K. Liu, and H. Lei, Large magnetoresistance in LaBi: Origin of field-induced resistivity upturn and plateau in compensated semimetals, New J. Phys. **18**, 082002 (2016).

[38] Y.-Y. Wang, Q.-H. Yu, P.-J. Guo, K. Liu, and T.-L. Xia, Resistivity plateau and extremely large magnetoresistance in $NbAs_2$ and $TaAs_2$, Phys. Rev. B **94**, 041103(R) (2016).

[39] F. Zwick, H. Berger, M. Grioni, G. Margaritondo, L. Forró, J. LaVeigne, D.B. Tanner, and M. Onellion, Coexisting one-dimensional and three-dimensional spectral signatures in $TaTe_4$, Phys. Rev. B **59**, 7762 (1999).

[40] B. Dardel, D. Malterre, M. Grioni, P. Weibel, Y. Baer, and F. Lévy, Unusual photoemission spectral function of quasi-one-dimensional metals, Phys. Rev. Lett. **67**, 3144 (1991).

[41] Y. Hwu, P. Almeras, M. Marsi, H. Berger, F. Lévy, M. Grioni, D. Malterre, and G. Margaritondo, Photoemission near the Fermi energy in one dimension, Phys. Rev. B **46**, 13624 (1992).

[42] I. R. Fisher, M. C. Shapiro, and J. G. Analytis, Principles of crystal growth of intermetallic and oxide compounds from molten solutions, Philos. Mag. **92**, 2401 (2012).

[43] See Supplemental Material at http://link.aps.org/supplemental/10.1103/PhysRevB.110.125151 for additiontal information on

(I) crystal structure and chemical composition of the $TaTe_4$ sample; (II) crystal structure of the high-symmetry phase ($1\times1\times1$) and the CDW phase ($2\times2\times3$) of $TaTe_4$; (III) determination of the inner potential V_0; (IV) polarization dependence of the ARPES spectra of $TaTe_4$; (V) effects of spin-orbit coupling in the DFT calculations of $TaTe_4$ in the non-CDW structure; (VI) Wannier calculations of the [001] and [100] surfaces.

[44] P. Hohenberg and W. Kohn, Inhomogeneous electron gas, Phys. Rev. **136**, B864 (1964).

[45] W. Kohn and L. J. Sham, Self-consistent equations including exchange and correlation effects, Phys. Rev. **140**, A1133 (1965).

[46] G. Kresse and J. Furthmüller, Efficient iterative schemes for *ab initio* total-energy calculations using a plane-wave basis set, Phys. Rev. B **54**, 11169 (1996).

[47] G. Kresse and D. Joubert, From ultrasoft pseudopotentials to the projector augmented-wave method, Phys. Rev. B **59**, 1758 (1999).

[48] P. E. Blöchl, Projector augmented-wave method, Phys. Rev. B **50**, 17953 (1994).

[49] J. P. Perdew, A. Ruzsinszky, G. I. Csonka, O. A. Vydrov, G. E. Scuseria, L. A. Constantin, X. Zhou, and K. Burke, Restoring the density-gradient expansion for exchange in solids and surfaces, Phys. Rev. Lett. **100**, 136406 (2008).

[50] H. J. Monkhorst and J. D. Pack, Special points for Brillouin-zone integrations, Phys. Rev. B **13**, 5188 (1976).

[51] D. Hobbs, G. Kresse, and J. Hafner, Fully unconstrained noncollinear magnetism within the projector augmented-wave method, Phys. Rev. B **62**, 11556 (2000).

[52] U. Herath, P. Tavadze, X. He, E. Bousquet, S. Singh, F. Muñoz, and A. H. Romero, PyProcar: A Python library for electronic structure pre/post-processing, Comput. Phys. Commun. **251**, 107080 (2020).

[53] A. A. Mostofi, J. R. Yates, G. Pizzi, Y.-S. Lee, I. Souza, D. Vanderbilt, and N. Marzari, An updated version of wannier90: A tool for obtaining maximally-localised Wannier functions, Comput. Phys. Commun. **185**, 2309 (2014).

[54] G. Pizzi, V. Vitale, R. Arita, S. Blügel, F. Freimuth, G. Géranton, M. Gibertini, D. Gresch, C. Johnson, T. Koretsune, J. I. nez Azpiroz, H. Lee, J.-M. Lihm, D. Marchand, A. Marrazzo, Y. Mokrousov, J. I. Mustafa, Y. Nohara, Y. Nomura, L. Paulatto *et al.*, Wannier90 as a community code: New features and applications, J. Phys.: Condens. Matter **32**, 165902 (2020).

[55] Q. Wu, S. Zhang, H.-F. Song, M. Troyer, and A. A. Soluyanov, WannierTools : An open-source software package for novel topological materials, Comput. Phys. Commun. **224**, 405 (2018).

[56] K. Momma and F. Izumi, *VESTA3* for three-dimensional visualization of crystal, volumetric and morphology data, J. Appl. Crystallogr. **44**, 1272 (2011).

[57] E. Bjerkelund and A. Kjekshus, On the crystal structure of $TaTe_4$, J. Less-Common Met. **7**, 231 (1964).

[58] B. Guster, M. Pruneda, P. Ordejón, and E. Canadell, Competition between Ta-Ta and Te-Te bonding leading to the commensurate charge density wave in $TaTe_4$, Phys. Rev. B **105**, 064107 (2022).

[59] S. Moser, An experimentalist's guide to the matrix element in angle resolved photoemission, J. Electron Spectrosc. Relat. Phenom. **214**, 29 (2017).

[60] A. F. Santander-Syro, O. Copie, T. Kondo, F. Fortuna, S. Pailhès, R. Weht, X. G. Qiu, F. Bertran, A. Nicolaou, A. Taleb-Ibrahimi, P. L. Fèvre, G. Herranz, M. Bibes, N. Reyren, Y. Apertet, P. Lecoeur, A. Barthélémy, and M. J. Rozenberg, Two-dimensional electron gas with universal subbands at the surface of $SrTiO_3$, Nature (London) **469**, 189 (2011).

[61] T. C. Rödel, F. Fortuna, S. Sengupta, E. Frantzeskakis, P. L. Fèvre, F. Bertran, B. Mercey, S. Matzen, G. Agnus, T. Maroutian, P. Lecoeur, and A. F. Santander-Syro, Universal fabrication of 2D electron systems in functional oxides, Adv. Mater. **28**, 1976 (2016).

[62] H. Zhang, C.-X. Liu, X.-L. Qi, X. Dai, Z. Fang, and S.-C. Zhang, Topological insulators in Bi_2Se_3, Bi_2Te_3 and Sb_2Te_3 with a single Dirac cone on the surface, Nat. Phys. **5**, 438 (2009).

[63] P. H. R. Gonçalves, L. Calil, I. Antoniazzi, T. Chagas, A. Malachias, E. A. Soares, V. E. Carvalho, D. R. Miquita, R. Magalhães-Paniago, and W. S. Silva, Experimental realization of a quaternary Bi-chalcogenide topological insulator with smaller effective mass, J. Phys. Chem. C **123**, 14398 (2019).

[64] T. Arakane, T. Sato, S. Souma, K. Kosaka, K. Nakayama, M. Komatsu, T. Takahashi, Z. Ren, K. Segawa, and Y. Ando, Tunable Dirac cone in the topological insulator $Bi_{2-x}Sb_xTe_{3-y}Se_y$, Nat. Commun. **3**, 636 (2012).

[65] Z. Wang, O. I. Malyi, X. Zhao, and A. Zunger, Mass enhancement in $3d$ and $s-p$ perovskites from symmetry breaking, Phys. Rev. B **103**, 165110 (2021).

[66] W. Ku, T. Berlijn, and C.-C. Lee, Unfolding first-principles band structures, Phys. Rev. Lett. **104**, 216401 (2010).

[67] P. Zhang, P. Richard, T. Qian, Y.-M. Xu, X. Dai, and H. Ding, A precise method for visualizing dispersive features in image plots, Rev. Sci. Instrum. **82**, 043712 (2011).

[68] J. Gooth, B. Bradlyn, S. Honnali, C. Schindler, N. Kumar, J. Noky, Y. Qi, C. Shekhar, Y. Sun, Z. Wang, B. A. Bernevig, and C. Felser, Axionic charge-density wave in the Weyl semimetal $(TaSe_4)_2I$, Nature (London) **575**, 315 (2019).

[69] W. Shi, B. J. Wieder, H. L. Meyerheim, Y. Sun, Y. Zhang, Y. Li, L. Shen, Y. Qi, L. Yang, J. Jena, P. Werner, K. Koepernik, S. Parkin, Y. Chen, C. Felser, B. A. Bernevig, and Z. Wang, A charge-density-wave topological semimetal, Nat. Phys. **17**, 381 (2021).

[70] S. Park and B.-J. Yang, Classification of accidental band crossings and emergent semimetals in two-dimensional noncentrosymmetric systems, Phys. Rev. B **96**, 125127 (2017).

[71] Y. Zhang, K. He, C.-Z. Chang, C.-L. Song, L.-L. Wang, X. Chen, J.-F. Jia, Z. Fang, X. Dai, W.-Y. Shan, S.-Q. Shen, Q. Niu, X.-L. Qi, S.-C. Zhang, X.-C. Ma, and Q.-K. Xue, Crossover of the three-dimensional topological insulator Bi_2Se_3 to the two-dimensional limit, Nat. Phys. **6**, 584 (2010).

[72] O. V. Yazyev, J. E. Moore, and S. G. Louie, Spin polarization and transport of surface states in the topological insulators Bi_2Se_3 and Bi_2Te_3 from first principles, Phys. Rev. Lett. **105**, 266806 (2010).

[73] Z. K. Liu, B. Zhou, Y. Zhang, Z. J. Wang, H. M. Weng, D. Prabhakaran, S.-K. Mo, Z. X. Shen, Z. Fang, X. Dai, Z. Hussain, and Y. L. Chen, Discovery of a three-dimensional topological dirac semimetal, Na_3Bi, Science **343**, 864 (2014).

[74] S.-Y. Xu, I. Belopolski, N. Alidoust, M. Neupane, G. Bian, C. Zhang, R. Sankar, G. Chang, Z. Yuan, C.-C. Lee, S.-M. Huang, H. Zheng, J. Ma, D. S. Sanchez, B. Wang, A. Bansil, F. Chou,

P. P. Shibayev, H. Lin, S. Jia *et al.*, Discovery of a Weyl fermion semimetal and topological Fermi arcs, Science **349**, 613 (2015).

[75] Z. K. Liu, J. Jiang, B. Zhou, Z. J. Wang, Y. Zhang, H. M. Weng, D. Prabhakaran, S.-K. Mo, H. Peng, P. Dudin, T. Kim, M. Hoesch, Z. Fang, X. Dai, Z. X. Shen, D. L. Feng, Z. Hussain, and Y. L. Chen, A stable three-dimensional topological Dirac semimetal Cd_3As_2, Nat. Mater. **13**, 677 (2014).

[76] A. A. Soluyanov and D. Vanderbilt, Wannier representation of $\mathbb{Z}_2$ topological insulators, Phys. Rev. B **83**, 035108 (2011).

[77] Y. Zhang, R. Zhou, H. Wu, J. S. Oh, S. Li, J. Huang, J. D. Denlinger, M. Hashimoto, D. Lu, S.-K. Mo, K. F. Kelly, G. T. McCandless, J. Y. Chan, R. J. Birgeneau, B. Lv, G. Li, and M. Yi, Charge order induced dirac pockets in the nonsymmorphic crystal $TaTe_4$, Phys. Rev. B **108**, 155121 (2023).